Alexandria Engineering Journal (2023) 68, 417–435

HOSTED BY

Alexandria University

Alexandria Engineering Journal

www.elsevier.com/locate/aej
www.sciencedirect.com

The investigation of the innovative hybrid heat pump system designed and prototyped for heating process of electric vehicles

Gökhan Sevilgen [a,*], Muhsin Kiliç [b], Halil Bayram [c], Enes Başak [a], Harun Dursun [a]

[a] Department of Automotive Engineering, Engineering Faculty, Bursa Uludağ University, Bursa, Turkey
[b] Department of Mechanical Engineering, Engineering Faculty, Bursa Uludağ University, Bursa, Turkey
[c] Department of Mechanical Engineering, Engineering Faculty, Amasya University, Amasya, Turkey

Received 1 September 2022; revised 11 October 2022; accepted 19 January 2023

KEYWORDS

Hybrid heat pump;
Driving range;
Heating process;
Electric vehicle;
CFD

Abstract In this paper, the investigation of the innovative hybrid heat pump system (HHPS) included Positive Temperature Coefficient (PTC) heater commonly used in electric vehicles (EVs) was performed in different heating modes to reach the desired temperature in a target time. The developed HHPS was evaluated in different heating modes in order to reach the desired temperature considering the both target time and also vehicle driving range. It was shown that the driving range can be increased up to 15 % by using HHPS. As a result, a high-capacity PTC heater and HP should be work together at the beginning of the heating, and then the PTC capacity should be reduced gradually at lower ambient conditions. Another important result is that HHPS represent a promising solution for the new generation EVs that the target temperature was obtained lower than 300 s at lower ambient conditions. A numerical model was also developed to investigate the flow and the thermal characteristics of the EV cabin interior that enable to design more effective heating, ventilation and air-conditioning (HVAC) systems of EVs under different environmental conditions and the numerical results were in good agreement with the experimental data used in this study.

© 2023 THE AUTHORS. Published by Elsevier BV on behalf of Faculty of Engineering, Alexandria University. This is an open access article under the CC BY-NC-ND license (http://creativecommons.org/licenses/by-nc-nd/4.0/).

1. Introduction

In EVs, PTC heaters were commonly used as a heating element that used high level of energy consumption from battery package in winter conditions and this lead to reduce battery life and also vehicle range in the long term. EV's driving range can be reduced up to 50 % with PTC electric heater due to its low heating efficiency [1]. Moreover, energy management of EVs, is a critical subject due to limitation of energy storage supplied by batteries [2,3]. So, the heating process has to be improved by using alternative systems such as HP or HHPS etc. [4–6]. The hybrid denotes using other heat sources together with HP system to improve the heating performance of system,

* Corresponding author.
E-mail address: gsevilgen@uludag.edu.tr (G. Sevilgen).
Peer review under responsibility of Faculty of Engineering, Alexandria University.

https://doi.org/10.1016/j.aej.2023.01.045
1110-0168 © 2023 THE AUTHORS. Published by Elsevier BV on behalf of Faculty of Engineering, Alexandria University.
This is an open access article under the CC BY-NC-ND license (http://creativecommons.org/licenses/by-nc-nd/4.0/).

Nomenclature

$\bar{T}$	: average temperature [°C]
U_j	: average velocity [m.s^{-1}]
$\bar{p}$	: average pressure [Pa]
S	: driving range [km]
S_E	: energy source term [kg.m^{-1}.s^{-3}]
k	: effective thermal conductivity [W.m^{-1}.K^{-1}]
T'	: fluctuating temperature [°C]
u_i'	: fluctuating velocity components [m.s^{-1}]
Q	: heat transfer rate [kW]
$\dot{m}$	: mass flow rate, [kg.s^{-1}]
S_m	: mass source [kg.m^{-3}.s^{-1}]
S_M	: momentum source [kg.m^{-2}.s^{-2}]
P	: pressure [Pa], vehicle battery capacity [kWh]
W	: power consumption [kW]
c_p	: specific heat at constant pressure, [J.kg^{-1}.K^{-1}]
T	: temperature [°C]
t	: time [h]
v	: vehicle speed [km.h^{-1}]

Greek letters

μ	: dynamic viscosity [kg.m^{-1}.s^{-1}]
ρ	: fluid density [kg.m^{-3}]

Subscripts

c	: coolant
i	: inlet
o	: outlet
t	: turbulence

Abbreviations

AC	: air conditioning
COP	: coefficient of performance
CAD	: computer-aided design
CFD	: computational fluid dynamics
cons.	: constant
EVs	: electric vehicles
Exp.	: experimental
HEX	: heat exchanger
HPS	: heat pump systems
HVAC	: heating, ventilation and air-conditioning
HHM	: high heating mode
HHPS	: hybrid heat pump system
MHM	: mixing heating mode
PCM	: phase-change material
PTC	: Positive Temperature Coefficient
cons.	: constant
var.	: variable

especially in cold weather conditions [7]. In EVs, the suitable heat sources that can be used for heating process are wasted heat of battery package, electric motor and other components but these sources are inadequate to meet the needs for driver and passengers' thermal comfort in different environmental conditions. In addition, thermal management of battery and electric motor cooling can be classified based on air, liquid, phase change materials, heat pipe and combination of these systems [8]. Among these methods, liquid cooling is commonly used for battery and motor applications because of high efficiency and easy maintenance [9–13]. In current literature, some researches based on using wasted heat of battery and electric motor to achieve the thermal comfort conditions were performed for EVs thermal management system and performance analysis [14–19,44]. Not only heating or cooling performance but also dehumidification function of HVAC system of an electric vehicle had to be considered for evaluation of energy consumption of EVs HVAC system running in different modes [45,46].On the other hand, a very limited studies on electric vehicles of HVAC systems in which both numerical simulations and experimental studies were presented together [47,48]. Whereas, there were mostly numerical or experimental studies included energy consumption of HP systems developed for EVs in the current literature. In this paper, both numerical and experimental results were presented for the evaluation of the energy consumption and also driving range to reach the desired temperature and the HVAC system not only meet the heating demand but also provide the thermal comfort conditions in a reasonable time period. Thus, the numerical simulation approach and the experimental method presented in this study will be utilized together to achieve the thermal comfort conditions in EVs considering energy consumption, driving range and also target time. Moreover, current studies in available literature were based on measurements on different EVs used in real life and the presented heating systems and the experimental results were specific to the EV used in these studies and there were a few studies based on vehicle cabin heating performance analysis in laboratory environment by using a generic electric vehicle cabin that can be used as a reference model in further studies [20]. In this study, a generic electric vehicle cabin located in an environmental chamber that provides the outdoor temperature range from −30 to 50 °C was used to analyze the heating performance of HHPS under different environmental conditions. Although R-134a is still a widely used refrigerant in vehicle AC systems, it will no longer be used because of today's legal regulations. The R1234yf refrigerant that is compatible with legal regulations of current vehicles and is more environmentally friendly was used in the developed HHPS. The experimental system provides the opportunity for developing different strategies for heating process that improve not only heating performance but also getting the results of the effect of using wasted heat, PTC and heat pump separately or together on energy consumption of EV on the driving range.

With the consideration given above, the novelty and the main contributions to the scientific literature of this research can be stated as follows; a generic vehicle cabin was firstly developed in laboratory environment by using average vehicle dimensions used for EV's heating performance of HVAC system based on HHPS system. By using the results of heating performance analysis, thermal management of EVs can be evaluated in terms of different modes of heating processes such as high heating mode (HHM) called as rapid heating and mixing heating modes (MHM) called as moderate or low speed

heating processes in different environmental conditions. This study also contributes to decrease of energy usage for HVAC processes that considerably affects the mileage of the vehicle and also life cycle of batteries.

2. Materials and methods

2.1. The description of HHPS and the experimental set-up

The schematic view of heating system for EVs developed in this study is shown in Fig. 1. The hybrid heat pump system composed of three sub-systems defined as the main air-conditioning heat pump (AC/HP) refrigerant system (I), two coolant systems for improving heating (II) and also cooling (III) processes. The main AC/HP system consists of an electrical scroll type compressor, two plate type heat exchangers; working as a condenser (HEX_1) and an evaporator (HEX_2), and a standard thermal expansion valve. During the heating and cooling processes both the first and second coolant circuits were activated but they worked in different flow paths which provided seven different working modes described in Table 1. This table also shows how the developed system works in other operating modes.

In these coolant circuits, two finned tube air heat exchangers (heater cores) for heating or cooling process of air, electrical heater added for utilizing of wasted heat of electric vehicle, two pumps for recirculating of coolant for heating or cooling processes, three three-way valves provided the flow path of heating and cooling processes, a radiator used for heat transfer between coolant and ambient air for getting desired temperature of coolant depended on the heating or cooling process, an additional plate type heat exchanger (HEX_3) which is

Table 1 Flow paths of refrigerant and coolant for different working modes.

Hybrid Heat Pump System Working Modes		
Coolant_Circuit_1	**Coolant_Circuit_2**	**The main AC/HP circuit**
H1) Heating (with HEX_3)		
10–11-12–13-15–16-17–18-19–20-21–22-9–10	23–24-25–26-27–28-29–30-31–23	1–2-3–4-5–6-7–8-1
H2) Heating process (without HEX_3)		
10–11-12–14-15–16-17–18-19–20-21–22-9–10	23–24-25–26-27–28-29–30-31–23	1–2-3–4-5–6-7–8-1
H3) Heating process (only used HEX_3)		
10–11-12–13-15–16-17–18-19–20-21–22-9–10	–	–
C1) Cooling process (with HEX_3)		
10–11-12–13-15–32-27–28-29–33-19–20-21–22-9–10	23–24-25–34-35–36-31–23	1–2-3–4-5–6-7–8-1
***C*2) Cooling process (without HEX_3)**		
10–11-12–14-15–32-27–28-29–33-19–20-21–22-9–10	23–24-25–34-35–36-31–23	1–2-3–4-5–6-7–8-1
D1) Defogging process		
10–11-12–13-15–16-17–18-19–20-21–22-9–10	23–24-25–34-35–36-31–23	1–2-3–4-5–6-7–8-1
D2) Deicing process		
10–11-12–14-15–16-17–18-19–20-21–22-9–10	23–24-25–34-35–36-31–23	1–2-3–4-5–6-7–8-1

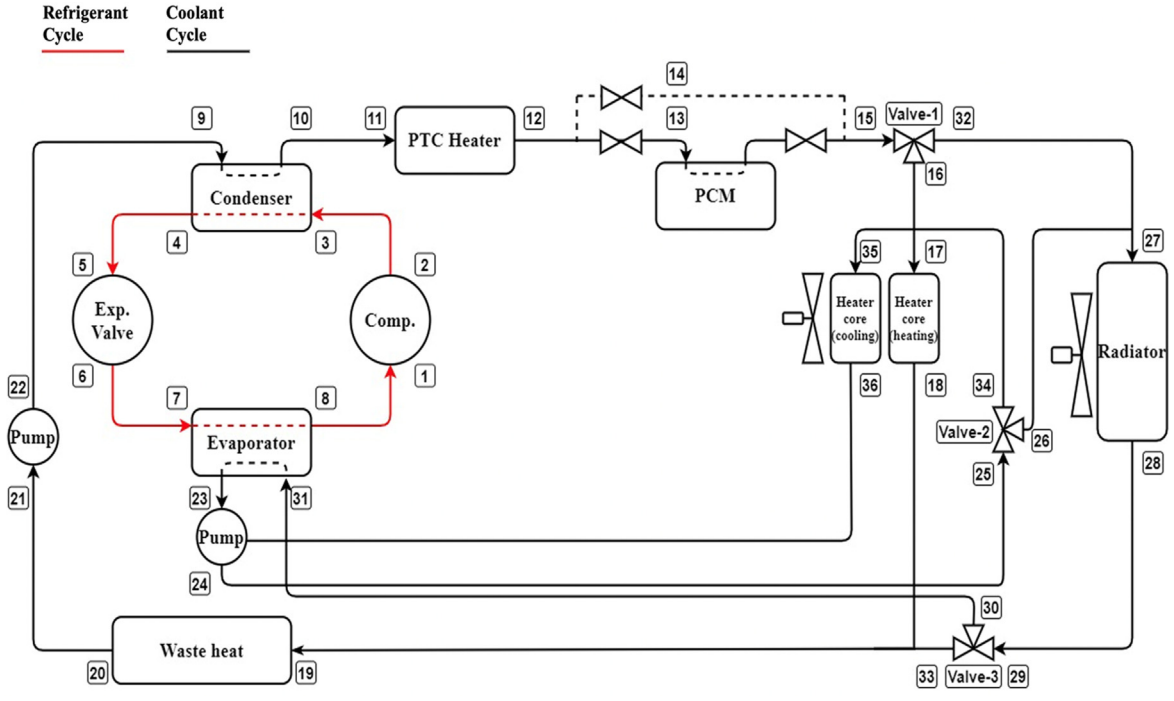


Fig. 1 The schematic view of HHPS developed in this study.

filled with phase-change material (PCM) that can be used for improving heating process by utilizing latent heat of PCM, three valves that activate the HEX_3 when utilizing latent heat of PCM material and a PTC heater that commonly used for heating process of current electric vehicles and these type of heaters influenced the electricity consumption and driving range significantly [5,21,22]. In the main AC/HP system, the refrigerant was selected as R1234yf which is compatible with legal regulations of current vehicles and is more environmentally friendly compared to the R-134a [23–25]. The coolant type was chosen as the mixture of water and ethylene–glycol with mass fraction of 50 % in both heating and cooling processes due to its capability to be used at winter conditions. The intersection region of the refrigerant and coolant cycles of the system shown in Fig. 2a was provided by plate type heat exchangers used as condenser and an evaporator in the main AC/HP system. In this study, only the second heating mode (H2) was investigated experimentally and the other four modes (H1, H3, C1 and *C*2 shown in Table 1) will not be presented and discussed in this paper. This paper focused on using the main AC/HP system with PTC heater for getting better conditions in terms of energy management and also improving driving range of EVs.

The properties of components used in the whole system are listed in Table 2. The electrical scroll type compressor had maximum 3 kW capacity, the condenser and evaporator used in the experiments were plate type of heat exchangers which had maximum 4 kW and 3 kW capacities, respectively. The environmental chamber used for getting different outdoor conditions of experiments is shown in Fig. 2b. The environmental chamber provided the outdoor temperature of the electric vehicle cabin between −30 °C and 50 °C. The environmental chamber had large enough to allow air-flow occurred from the outer surfaces of the electric vehicle cabin and the dimensions of this chamber is shown in Fig. 2c. The inner components used in the environmental chamber are shown in Fig. 2d. These components are electric vehicle cabin, AC/HP system and radiator fan that can be controlled for providing vehicle speed depends on the selected driving cycle. All driving cycles can be simulated in the environmental chamber by using software interface developed in this study, however, wasted heat depends on driving cycle that improve the heating process will be taken account in further studies. In the experiments, the interior surfaces of the electric vehicle cabin be demonstrated in Fig. 2e.

The electric vehicle cabin was designed and manufactured by using real dimensions of a car in 1:1 scale considering similar studies performed in current literature and international automotive standards [26–29]. There was an air duct system made of flexible material between heater cores and inlet vents that provide the air flow needed in the heating/cooling processes to the electric vehicle cabin interior environment.

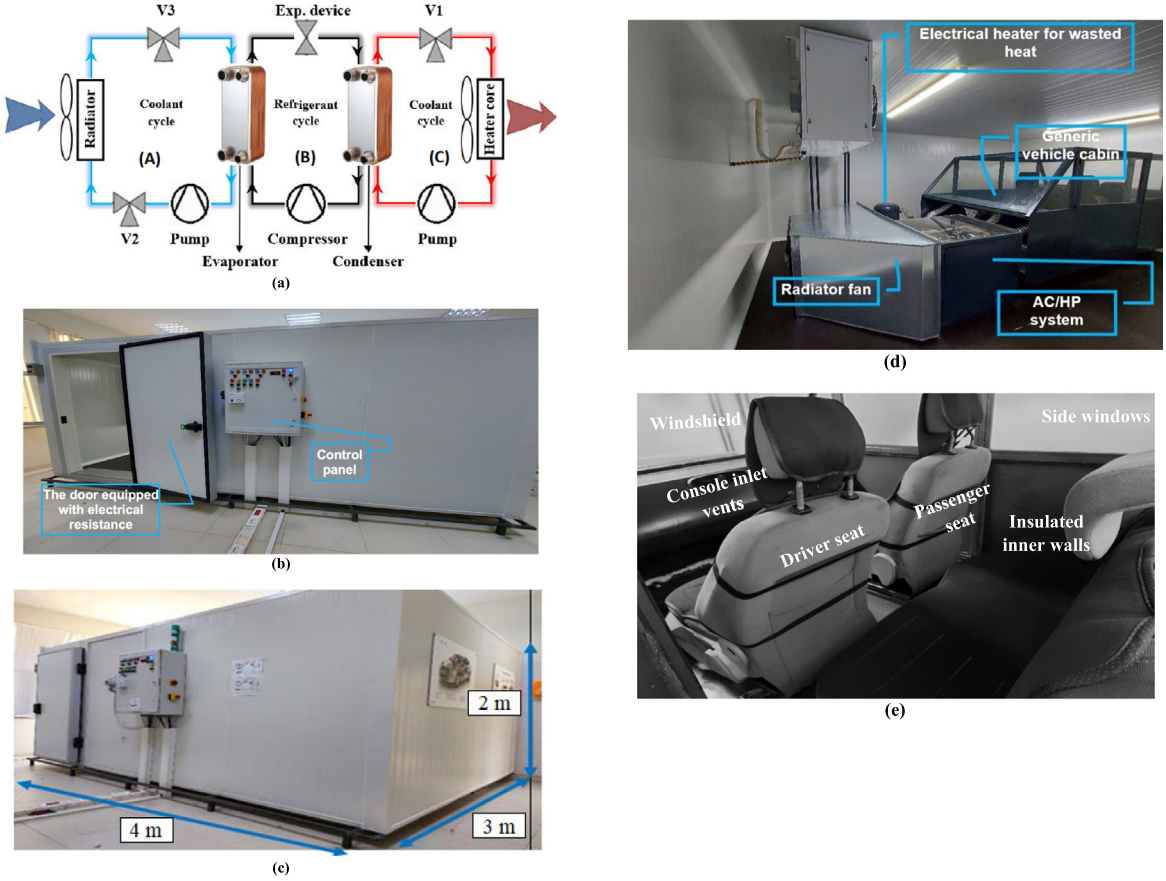


Fig. 2 **(a)** The intersection region of the refrigerant and coolant circuits developed in this study **(b)** the environmental chamber and **(c)** the dimensions of this chamber used in the experiments **(d)** the main components used in the environmental chamber **(e)** the interior surfaces of the electric vehicle cabin.

Table 2 The properties of components used in the refrigerant and coolant circuits.

Circuit	Type	Properties
AC/HP circuit	Scroll type compressor	Capacity: 3.0 kW
	Plate type condenser (HEX_1)	Flow condition: parallel flow Plate number: 32 Capacity: 4.0 kW
	Plate type evaporator (HEX_2)	Flow condition: parallel flow Plate number: 24 Capacity: 3.0 kW
	Thermal expansion valve	10 kW
	The electrical heater for wasted heat	max. 6.0 kW
	The PTC heater	max. 4.5 kW
Coolant circuits	Pump_1(condenser side)	Mass flow rate: 0.03 kg/s
	Pump_2(evaporator side)	Mass flow rate: 0.06 kg/s
	Three-way valves	Suitable for vehicle
	Radiator	Finned tube HEX
	Heater cores (heating or cooling)	Finned tube HEX
The environmental chamber	The metal surfaces filled with polyurethane insulation material	Temperature range: −30 °C to 50 °C
Vehicle cabin	Produced with sheet metal	Insulated inner surfaces

The air duct system provides the necessary air-flow to the interior of the vehicle cabin through console, floor and defroster type of vents, as in real vehicles. In this way, the effect of the use of different inlet vents, and therefore of different air-flow characteristics, on the air temperature of the interior of the vehicle cabin will be examined. In this study, the console vents were only used in the experimental study. The air duct system and all other related components (PTC heater, wasted heat simulator, etc.) were thermally insulated to minimize the thermal losses. The main dimensions of vehicle cabin and the surface area of this electric vehicle cabin are listed in Table 3.

Table 3 The geometric properties of the electric vehicle cabin used in the experiments.

The dimensions of vehicle cabin (m)	
Width:	1.50
Length:	2.29
Height:	1.30
The outer surface areas of the vehicle cabin (m^2)	
Top surface	2.66
Floor surface	3.44
The left side of the vehicle cabin	1.94
The right side of the vehicle cabin	1.94
Windshield	0.92
The right window (front side)	0.44
The right window (rear side)	0.43
The left window (front side)	0.44
The left window (rear side)	0.43
The rear window	0.74

2.2. The measurement devices and data acquisition system used in the experimental study

The measurement devices, measuring ranges and accuracy of each devices used in the experiments are listed in Table 4. In AC/HP system the pressure and temperature measurements at the inlet and outlet sections of each components were carried out by using pressure transducers and temperature sensors which were PT100 type which had different connection elements and accuracy. The first type of PT100-RTR was used in the AC/HP and coolant circuits and the second type of PT100-RTS was used for temperature measurements in the electric vehicle cabin. The velocity measurement near the inlet vents were performed by using anemometer. The measurement of volumetric flow rate of coolant in heating and cooling circuits was achieved by using two flowmeters and the flow rate of coolant for each circuit can be controlled in three stages. The locations of measurement points in the whole HP system are shown in Fig. 3a.

The data acquisition system allows that all the pressure and temperature measurements were recorded and monitored instantly by using a control panel included Wi-Fi modem and automation card that transfers the experimental data by

Table 4 The measurement devices accommodated in the experimental study.

AC/HP and Coolant circuits		
Type of device	Measuring range	Accuracy
Pressure transducer	0–50 bar	± 0.05 bar
Temperature sensor (PT100-RTR)	−50 °C / + 400 °C	± 0.01 °C
Flowmeter with	0.05–5.00 m^3/h	± 1.0 %
Internal temp. sensor (PT1000)	5 °C / 90 °C	± 0.1 °C
Electric vehicle cabin		
Type of device	Measuring range	Accuracy
Anemometer	0–30 m/s	± 0.05 m/s
Temperature sensor (PT100-RTS)	−25 °C / + 200 °C	± 0.01 °C
Environmental chamber		
Type of device	Measuring range	Accuracy
Relative humidity device	10 % / 99 %	± 1.0 %
Temperature sensor (PT100-RTR)	−50 °C / + 400 °C	± 0.01 °C

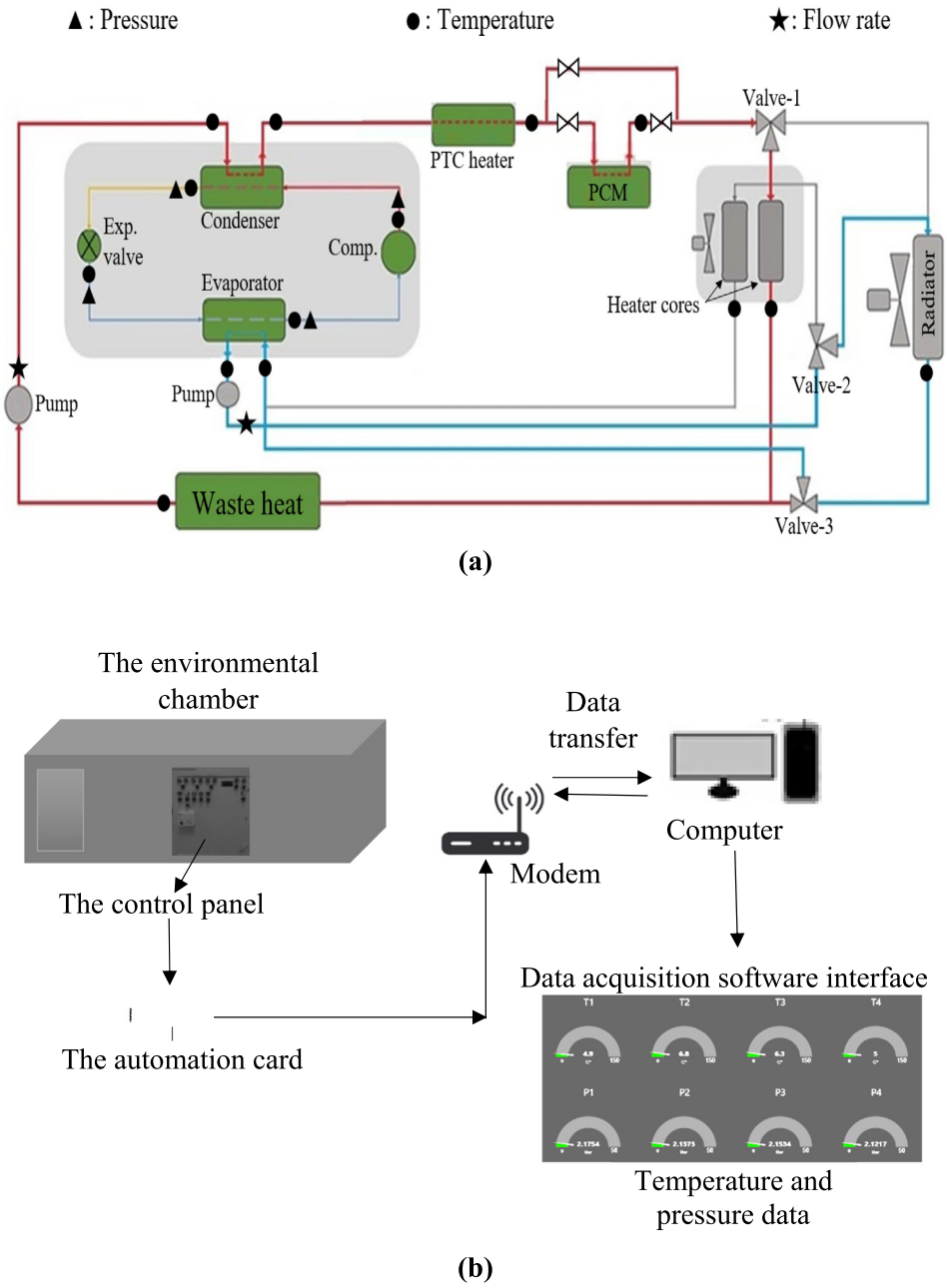


Fig. 3 **(a)** The locations of temperature, pressure and flow rate measurement points used in the experimental system and **(b)** the data acquisition system used in the experiments.

using acquisition software interface to the computer hard disc shown in Fig. 3b. The flow rate of coolants used in the heating and cooling circuits were directly monitored by using flow rate measurement device.

The experiments were performed in terms of using different heating sources such as PTC heater and HP system. In the experiments, the heating process was evaluated as high heating mode (HHM) and two different mixing heating modes (MHM) considered energy consumption of the whole system developed in this study. The MHM used in the experiments demonstrated in Fig. 4a and Fig. 4b. In the first mixing heating mode (MHM_1), the PTC_cons. heater had constant heating capacity ranged up to 3.5 kW during all heating process and the PTC_var. demonstrates the variable heating capacity decreased gradually from 3.5 kW to 1.0 kW in the second mixing heating mode (MHM_2) so that the minimizing PTC heater capacity and also reducing the total time of usage of this heater. These values have been determined by considering the studies that PTC heaters are used for heating electric vehicles [17,30].

In Fig. 4a to Fig. 4c, Δt_1 denotes the waiting time to make sure the starting temperature is equal to the initial temperature that was selected for each experiment and this time was about 10 s for all heating processes, T_{init} denotes the initial tempera-

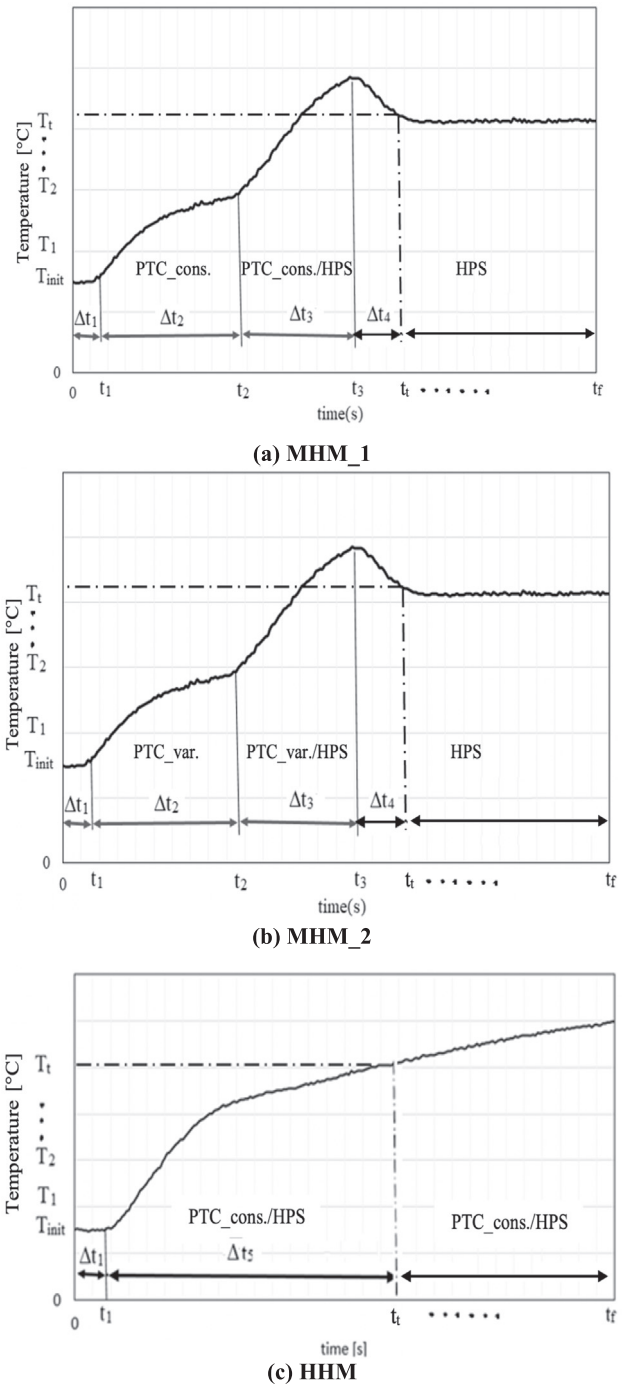


Fig. 4 The heating modes of developed HHPS for electric vehicle cabin; **(a)** The working principle of MHM_1, **(b)** MHM_2 and **(c)** HHM heating processes.

ture of the electric vehicle cabin interior, T_t denotes the target temperature value reached by the time t_t and t_f denotes the total time period of the heating process.

In the first mixing heating mode (MHM_1), the only PTC_cons. heater got started for heating process and the PTC_cons. heater worked in progress for Δt_2 time period, after this heating process, the HPS integrated with PTC heater and worked together for Δt_3 time period and finally the HP system met the heating demand of electric vehicle cabin alone for Δt_4 time period to meet the target temperature value (t_t). In the second heating mode (MHM_2), the variable heating capacity decreased gradually so that the decreasing the usage of PTC heater. Finally, in the heating mode of HHM demonstrated in Fig. 4c, the PTC heater with constant capacity was integrated with HPS system or the PTC heater was only utilized for heating process as used in current EVs.

In the experiments, these heating modes were determined by minimizing using of PTC heater as much as possible to optimize the energy consumption of whole system that increase the driving range of electric vehicle. The experiments performed for different heating modes were listed in Table 5, Tables 6 and 7.

For the evaluation of whole system performance, the COP values of the system were calculated by using Equations (1) and (2), according to whether the PTC heater is inactive or active, respectively [30]. Where, Q_h is the heat dissipated by the condenser and Q_{PTC} is the heat supplied by the PTC heater. The W_{PTC} and the W_{HP} represents the PTC and the compressor power consumption, respectively.

$$COP_h = \frac{Q_h}{W_h} \tag{1}$$

$$COP_{total} = \frac{Q_{total}}{W_{total}} = \frac{Q_h + Q_{PTC}}{W_h + W_{PTC}} \tag{2}$$

where, Q_h is the heat transfer rate (kW) which is the useful heat supplied by the plate type condenser and can be calculated for the coolant side by using Equation (3), where $\dot{m}_c$ is the mass flow rate (kg/s) of coolant, $c_{p,c}$ is the specific heat (kJ/kgśK) and $T_{c,i}$ (K) and $T_{c,o}$ (K) are the inlet and outlet temperature values of coolant defined for the entering and the leaving sections of the plate type condenser during heating process.

$$Q_h = \dot{m}_c c_{p,c}(T_{c,o} - T_{c,i}) \tag{3}$$

The relation between the energy reduction of the different heating modes and the driving range can be evaluated by using Equations (4)–(6), where, S is the driving range, t (h) is the time for which the cabin does not require heating. v (km/h) is the vehicle speed, and the P (kWh) is the vehicle battery capacity. For the evaluation of energy consumption in terms of driving range at the end of the heating process, the vehicle battery capacity and speed were assumed as 25 kWh and 60 km/h, respectively, considering the similar studies from the literature [31].

$$S_{PTC} = \frac{P.v}{\frac{P}{t} - W_{PTC}} \tag{4}$$

$$S_{HP} = \frac{P.v}{\frac{P}{t} - W_{HP}} \tag{5}$$

$$S_{HHPS} = \frac{P.v}{\frac{P}{t} - (W_{HP} + W_{PTC})} \tag{6}$$

2.3. The numerical study

The finite volume method was employed to perform the transient numerical calculations of the airflow and temperature fields of EV cabin interior by using ANSYS Fluent and the three-dimensional computer-aided design (CAD) model of

Table 5 The experiments performed for different ambient conditions by using MHM_1 heating modes of HHPS developed in this study.

	$T_{ambient}$ = -5°C / 0 °C / 5 °C				
	(Δ: *HP active (1.6 kW)* —: *HP passive*)				
Experiments and Heating Mode	**Heating source**	**Time (minutes)**			
		0–5 min.	**5–10 min.**	**10–15 min**	**15–20 min**
		Heater capacity			
Exp.1_MHM_1	PTC_cons.	3.0 kW	3.0 kW	3.0 kW	—
	HP	—	Δ	Δ	Δ
Exp.2_MHM_1	PTC_cons.	3.0 kW	3.0 kW	—	—
	HP	—	Δ	Δ	Δ
Exp.3_MHM_1	PTC_cons.	2.0 kW	2.0 kW	2.0 kW	—
	HP	—	Δ	Δ	Δ
Exp.4_MHM_1	PTC_cons.	2.0 kW	2.0 kW	—	—
	HP	—	Δ	Δ	Δ
Exp.5_MHM_1	PTC_cons.	3.0 kW	3.0 kW	—	—
	HP	—	—	Δ	Δ

Table 6 The experiments performed for different ambient conditions by using MHM_2 heating modes of HHPS developed in this study.

$T_{ambient}$ = -5°C / 0 °C / 5 °C					
(Δ: *HP active (1.6 kW)* —: *HP passive*)					
Experiments and Heating Mode	**Heating source**	**Time (minutes)**			
		0–6 min.	**6–12 min.**	**12–15 min**	**15–20 min**
		Heater capacity			
Exp.1_MHM_2	PTC_var.	3.5 kW	3.0 kW	2.5 kW	1.5 kW
	HP	—	—	Δ	Δ
Exp.2_MHM_2	PTC_var.	3.5 kW	3.5 kW	3.0 kW	2.5 kW
	HP	—	Δ	Δ	Δ
Exp.3_MHM_2	PTC_var.	3.5 kW	2.5 kW	1.5 kW	0.5 kW
	HP	—	Δ	Δ	Δ

the vehicle used in this study is shown in Fig. 5a. The mesh domain of the computational domain was very important for obtaining accurately predicted results and reducing the computing time and in the numerical calculations, hexahedral elements were used which are shown in Fig. 5b [32,33]. In the computational domain, about one million cells were generated for the transient heating simulation and the boundary conditions were determined considering experimental data. In transient numerical simulations, the initial boundary conditions are very important to get the precise numerical results. The initial and boundary conditions used in this numerical study were performed as the similar conditions of experiment of MHM_2 heating mode of HHPS. The boundary conditions that the initial ambient conditions were chosen as 5 °C and the transient temperature data measured near the inlet vents for 1200 s of heating period are shown in Fig. 5c and Fig. 5d.

The velocity magnitude was set to as a constant value of 2.5 m/s for all inlet vents which was obtained from the experiment and the direction of the resultant velocity vector was normal to the surface boundary in the numerical calculations. There were two different inlet vent(s); the first one is console type inlet vent(s) (M1), and the second one is defrost type inlet vent(s) (M2). In both numerical and experimental study, the console inlet vents were only used which were shown in Fig. 6a Atmospheric conditions were applied at the outlet surface. In the numerical simulations, convective boundary condition was considered at the outer surfaces of the cabin. In transient calculations, the time step was chosen as one second and was gradually increased depends on the convergence criterion that the normalized residuals of the continuity and momentum equations were less than 10^{-6} and the energy equation was less than 10^{-8}. The RNG k-ε model was chosen for the numerical calculations which was generally used for such calculations due to stability and precision of numerical results in the available literature [28,34–37].

The governing equations of the present study include continuity, momentum and energy conservation equations can be written for turbulent flow in equations (7)-(10).

Table 7 The experiments performed for different ambient conditions by using HHM heating modes of HHPS developed in this study.

$T_{ambient}$ = -5°C / 0 °C / 5 °C					
(Δ: *HP active (1.6 kW)* —: *HP passive*)					
Experiments and Heating Mode	**Heating source**	**Time (minutes)**			
		0–5 min.	**5–10 min.**	**10–15 min**	**15–20 min**
		Heater capacity			
Exp.1_HHM	PTC_cons.	3.0 kW	3.0 kW	3.0 kW	3.0 kW
	HP	—	Δ	Δ	Δ
Exp.2_HHM	PTC_cons.	3.0 kW	3.0 kW	3.0 kW	3.0 kW
	HP	—	—	Δ	Δ
Exp.3_HHM	PTC_cons.	2.0 kW	2.0 kW	2.0 kW	2.0 kW
	HP	—	Δ	Δ	Δ
Exp.4_HHM	PTC_cons.	2.0 kW	2.0 kW	2.0 kW	2.0 kW
	HP	—	—	Δ	Δ
Exp.5_HHM	PTC_cons.	3.0 kW	3.0 kW	3.0 kW	3.0 kW
	HP	Δ	Δ	Δ	Δ
Exp.6_HHM	PTC_cons.	2.0 kW	2.0 kW	2.0 kW	2.0 kW
	HP	Δ	Δ	Δ	Δ
Exp.7_HHM	PTC_cons.	3.0 kW	3.0 kW	3.0 kW	3.0 kW
	HP	—	—	—	—
Exp.8_HHM	PTC_cons.	2.0 kW	2.0 kW	2.0 kW	2.0 kW
	HP	—	—	—	—

$$\frac{\partial(\rho)}{\partial t}+\frac{\partial(\rho\overline{U_j})}{\partial x_j}=S_m \tag{7}$$

Equation (7) is the general form of the mass conservation equation, where, ρ is the fluid density, $\overline{U_j}$ is the average velocity, S_m is the mass source.

$$\frac{\partial(\rho\overline{U_i})}{\partial t}+\frac{\partial(\rho\overline{U_i}\overline{U_j})}{\partial x_j}=-\frac{\partial\bar{p}}{\partial x_i}+\frac{\partial}{\partial x_j}\left[\mu\frac{\partial\overline{U_i}}{\partial x_j}-\rho\overline{u_i'u_j'}\right]+S_M \tag{8}$$

Conservation of momentum is given in Equation (8), where, $\bar{p}$ is the average pressure, μ is the dynamic viscosity, S_M is the momentum source, $u_i'u_j'$ fluctuating velocity components and Reynolds stress tensor $\rho\,\overline{u_i'u_j'}$ must be modelled by applying turbulence models include turbulent viscosity (μ_t).

The energy equation can be written in the following form.

$$\rho c_p\frac{\partial\bar{T}}{\partial t}+\rho c_p\overline{U_i}\frac{\partial\bar{T}}{\partial x_i}=\frac{\partial}{\partial x_i}\left[k\frac{\partial\bar{T}}{\partial x_i}-\rho c_p\overline{u_i'T'}\right]+S_E \tag{9}$$

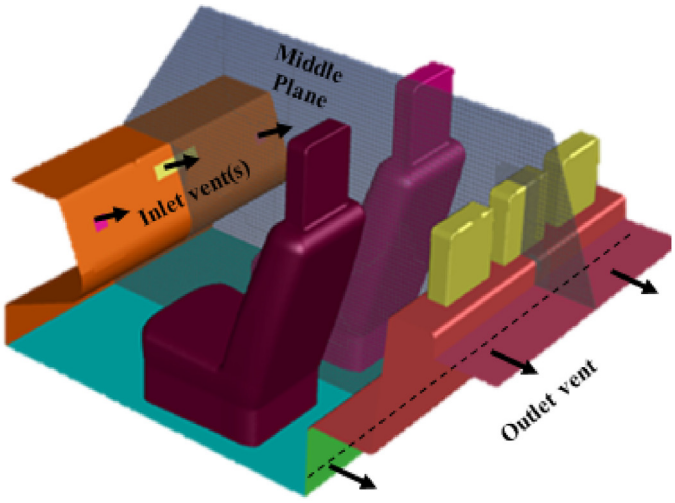
Where c_p is the specific heat, $\bar{T}$ and T' are the average and fluctuating temperature, respectively k is the effective thermal conductivity and S_E is the energy source term. The detailed information about these equations can be found in reference [33,38].

2.4. Validation of the numerical results

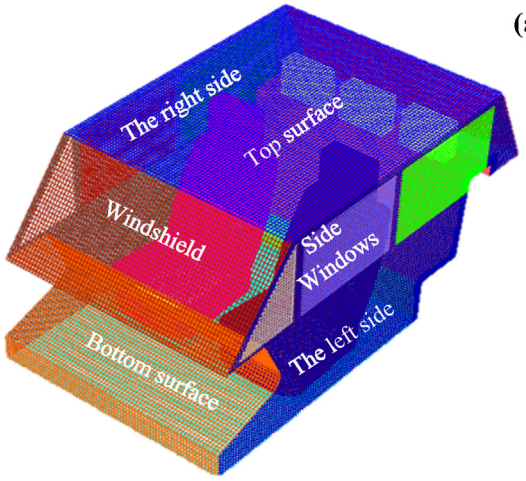
The locations of the measurement points used in the electric vehicle cabin for getting temperature data is shown in Fig. 6a and Fig. 6b. *P*1, *P*2, *P*3 and *P*4 were located in the front region of the vehicle cabin, however, P5, *P*6 and P7 were located in the back region of the vehicle cabin. In general, the interior volume of the automobiles is quite small compared to other air-conditioning applications, and the ratio of the volume occupied by individuals to the total volume in automobiles is relatively larger than the ratio in rooms and similar indoor environments. On the other hand, considering the thermal comfort and standards in closed spaces, while there are international standards for offices, and other closed spaces [39]. However, there is no general standard for the interior of the automobile cabin for the evaluation of the processes of HVAC system, so in this study, the locations of these points were determined considering similar studies mentioned in the available literature [40–42].

Comparative results of the experimental data and the calculated temperature values were demonstrated in Fig. 6c-6f. It can be seen from the results at the selected points (*P*1 to P7), the differences between the predicted and measured temperature data are about 2 °C in general. Another important result is that both the measured and computed temperature data curves presented same trend with the time. The temperature values obtained from the experimental study were slightly lower than the values of the numerical simulation because the heat losses from the outer surfaces of the vehicle cabin in the experimental study were higher than the developed numerical model. Considering the parameters such as heat losses from the outer surfaces of the cabin, heat transfer coefficient at the outer side, turbulent air-flow etc., there were too many factors affecting the numerical results. Hence, the predicted results can be accepted as very good with confidence.

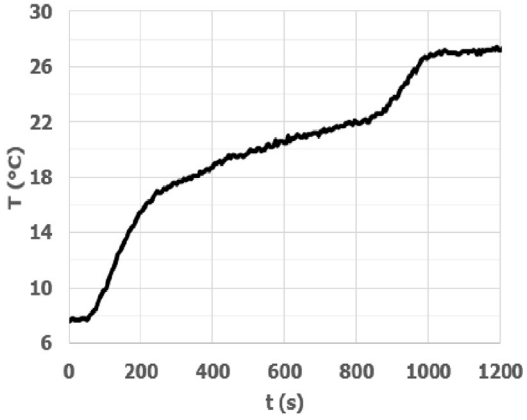
The *P*1 which located on the front region of vehicle cabin was selected for mesh independency analysis because the temperature gradients were highly changed near the inlet vent(s) and the numerical results of mesh independency analysis are shown in Fig. 6g. From these results of mesh independency analysis, it was found that about one million elements in total were enough for the temperature predictions.



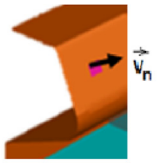
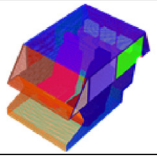
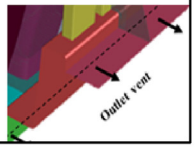
(a)



(b)



(c)

Inlet Vent(s) **Momentum :** $-V_n$ (Velocity) : 2.5 m/s **Heat Transfer :** $-T_{inlet} = T(t)$ (Fig.5c) (Transient inlet temperature boundary condition)	
Outer surfaces of the vehicle cabin shown in Fig.5b Convection boundary conditions used **Ambient temperature:** $T_{amb} = 5°C$	
Outlet Vent(s) **Momentum :** - Gauge Pressure : 0 Pa (Atmospheric conditions)	

(d)

Fig. 5 **(a)** The view of the generated CAD model and **(b)** the mesh structure of the vehicle cabin **(c)** Transient temperature data of inlet vents used in the numerical calculations (d) Boundary conditions used in the numerical calculations.

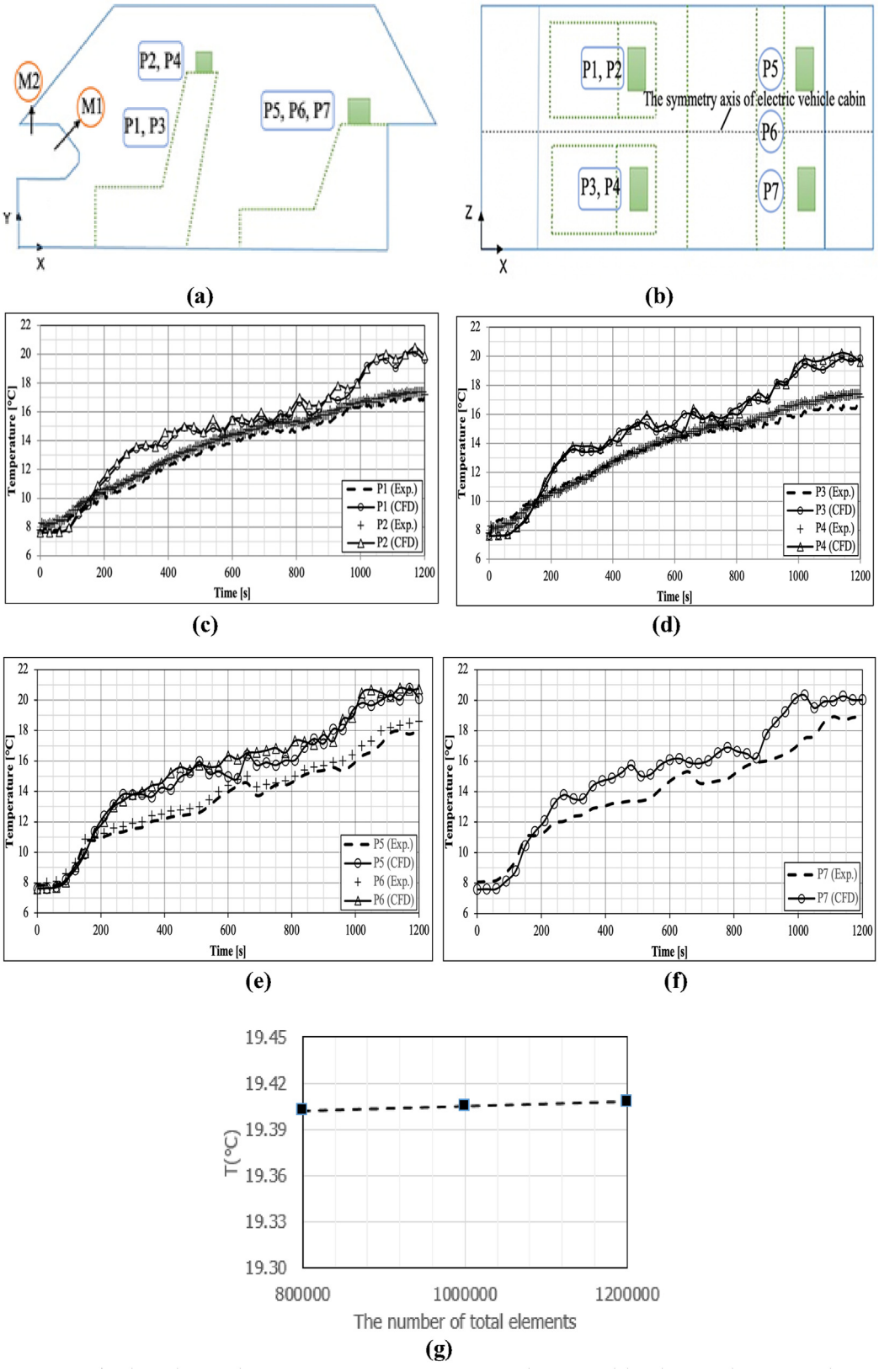


Fig. 6 The locations of temperature measurement points **(a)** side view and **(b)** top view of the electric vehicle cabin, Prediction of the temperature values and the comparison with the experimental data for **(c)** *P*1 and *P*2, **(d)** *P*3 and *P*4, **(e)** P5 and *P*6, **(f)** P7, **(g)** The numerical results of mesh independency analysis.

2.5. The theoretical calculations and uncertainty analysis

In order to determine the total experimental error, uncertainty analysis was carried out by using Equation (10) proposed by Moffat [43], where Δ symbol represents the accuracy of each measurement device used for temperature, pressure and flow rate measurements. *T, v, P and ṁ* represents the measured temperature, velocity, pressure and mass flow rate values during the experiments.

$$Totalerror(\%) = \left[\left(\frac{\Delta v}{v}\right)^2 + \left(\frac{\Delta T}{T}\right)^2 + \left(\frac{\Delta P}{P}\right)^2 + \left(\frac{\Delta \dot{m}}{\dot{m}}\right)^2 + \left(\frac{\Delta t}{t}\right)^2\right]^{\frac{1}{2}} \quad (10)$$

Δt denotes the time interval of measurement device, and the *t* represents the total time. The highest uncertainty in experimental data was calculated to be within ± 3 %.

3. Results and discussion

The temperature measurements obtained for different heating modes were evaluated in terms of both the time for getting target temperature and also energy consumption that affects the vehicle driving range. Thus, the calculated COP values by using Eqs.1–2 for different ambient conditions were presented in Fig. 7.

In the heating mode of MHM_1, the target temperature value was just obtained for the MHM_1 Exp_1 experiment at the end of the 1200 s heating period and the calculated vehicle driving range was decreased to 77 % for this experiment. The calculated COP values of this experiment shown in Fig. 7 was about 2.02 and this experiment had better results in terms of the time for getting target temperature and also energy consumption that affected the driving range in the heating mode of MHM_1.

The temperature values obtained from the experiments of heating mode of MHM_1 and the calculated vehicle driving range values for T = -5°C ambient temperature condition were shown in Fig. 8a and Fig. 8b, respectively.

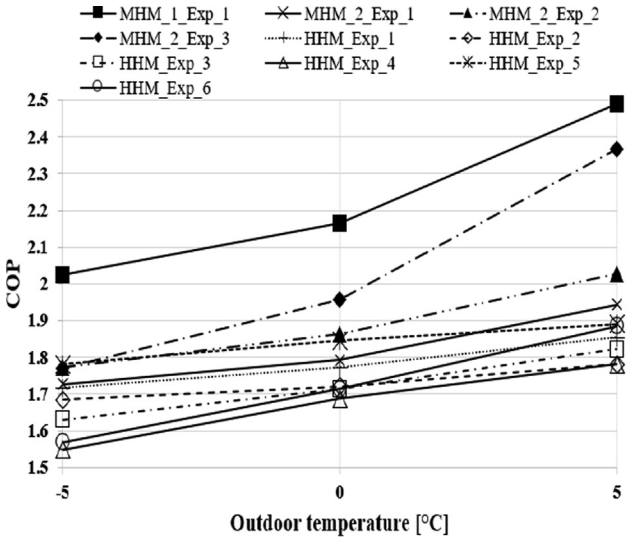


Fig. 7 The calculated COP values of the cases reached the target temperature at −5°C ambient temperature condition.

The temperature values obtained from the experiments of heating mode of MHM_2 and the calculated vehicle driving range values for T = -5°C ambient temperature condition were shown in Fig. 9a and Fig. 9b, respectively. In the heating mode of MHM_2, all experiments provided the target temperature after 1200 s heating period, however, in the experiments of MHM_2_Exp_1, the targeted temperature value was achieved about 900 s and this time period was longer than the other experiments of this heating mode. In the experiment of MHM_2_Exp3 the vehicle driving range reduced to 80 %, and the COP value was calculated about 1.77. However, in the experiment of MHM_2_Exp2, the measured temperature values were about 28 °C and this value was considerably exceeding the target temperature value and the driving range was dramatically reduced to 73.6 %. From the results of this heating mode, MHM_2_Exp_3 had better performance considering energy consumption and also vehicle driving range.

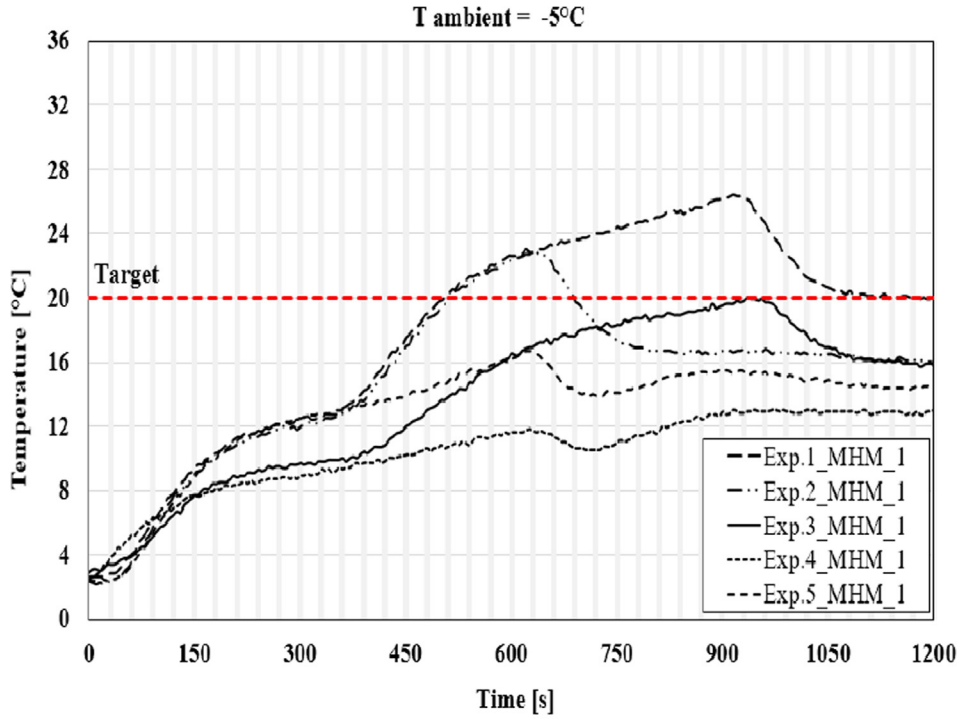
From the comparison of the experimental results of MHM_1 and MHM_2 heating modes, MHM_2_Exp_3 had better performance in terms of driving range and had similar COP value compared to the experiment of MHM_1_Exp1. On the other hand, in the experiment of MHM_1_Exp1, the temperature decrease was about 6 °C when the PTC heater was inactivated in the last five minutes of heating period and this reduction lead to problems for the heating process. Whereas, in the experiment of MHM_2_Exp2, the PTC heater was run constantly with HP system after five minutes of heating period but the heating capacity of this component was reduced gradually that leads to decrease in temperature and this value was about 4 °C. Thus, MHM_2_Exp_3 can be preferred for heating process especially at lower ambient temperature conditions while considering driving range and energy consumption.

The temperature values obtained from the experiments of heating mode of HHM and the calculated vehicle driving range values for T = -5°C ambient temperature condition were shown in Fig. 10a, Fig. 10b and Fig. 10c, respectively. From the results of these experiments, the temperature was constantly increased during the heating period for all experiments.

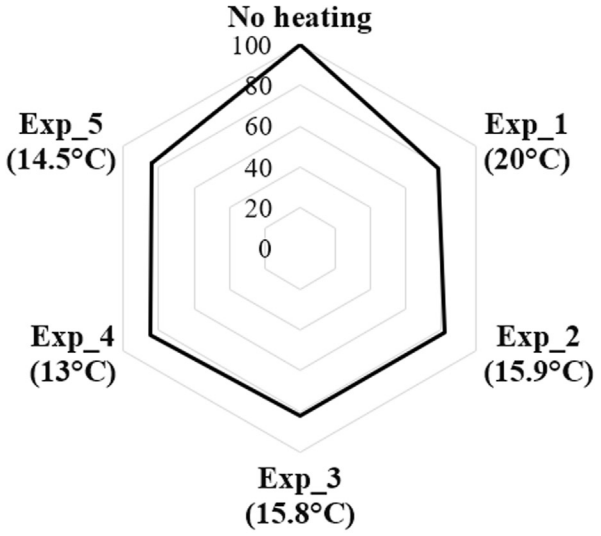
In the experiment of HHM_Exp_1, the target temperature was reached in about 500 s, and at the end of the experiment, the temperature was measured about 29 °C, which is quite higher than the target temperature. However, the COP value of this case was calculated about 1.69 and the vehicle driving range was reduced to 71 % in this heating mode. In the experiment of HHM_Exp_2, the target temperature had been reached with a delay of 4 min compared to the experimental results of the experiment of HHM_Exp_1.

In the experiment of HHM_Exp_3, the target temperature value was obtained about 750 s and the temperature value obtained at the end of the heating process was about 24 °C in this experiment.

In the experiment of HHM_Exp_4 case, where the minimum decrease in driving range was observed and the temperature value was obtained about 22 °C at the end of the heating period. However, it was determined that the time to reach the target temperature in this case was approximately 900 s. The calculated COP value was about 1.54 and the driving range was calculated for this experiment about 81.3 %.

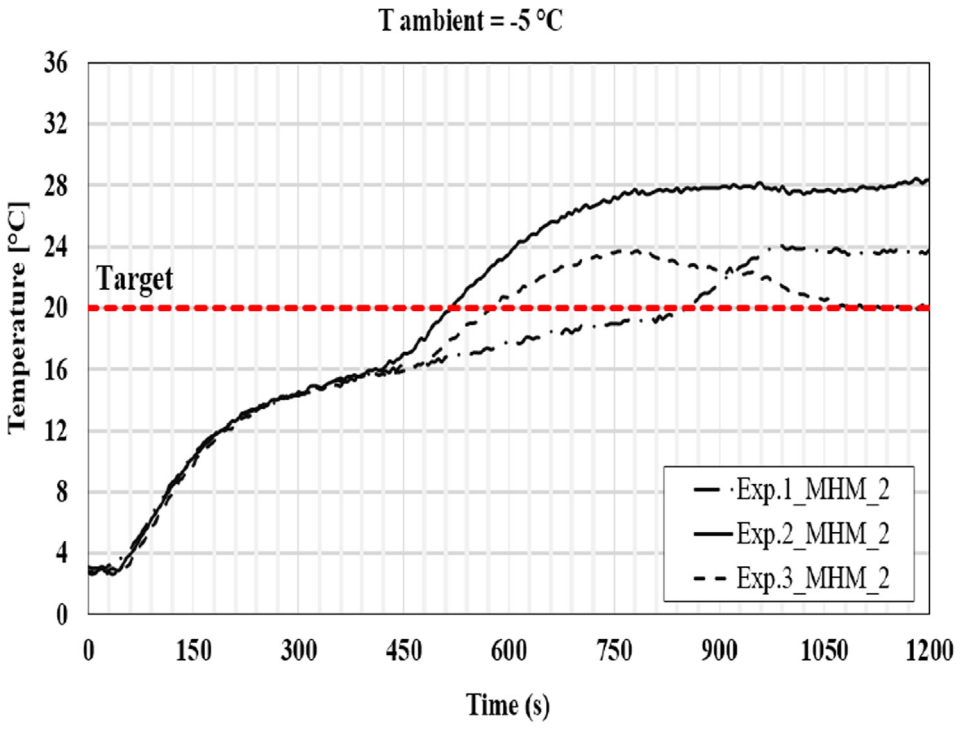


(a)

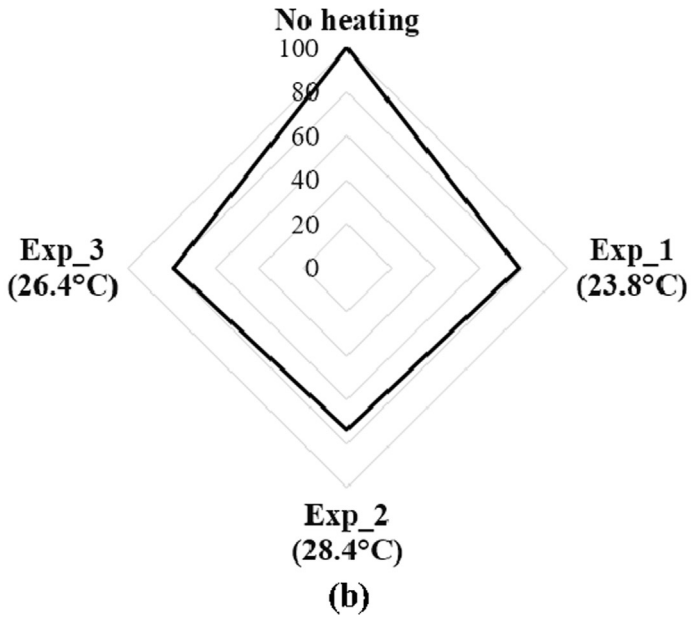


(b)

Fig. 8 **(a)** The temperature measurement data obtained for heating mode of MHM_1 at $T_{ambient}$ = -5 °C **(b)** The calculated vehicle driving range and the measured temperature values at 1200 s of the heating period for heating mode of MHM_1.



(a)



(b)

Fig. 9 **(a)** The temperature measurement data obtained for heating mode MHM_2 at $T_{ambient}$ = -5 °C **(b)** The calculated vehicle driving range and the measured temperature values at 1200 s of the heating period for heating mode of MHM_2.

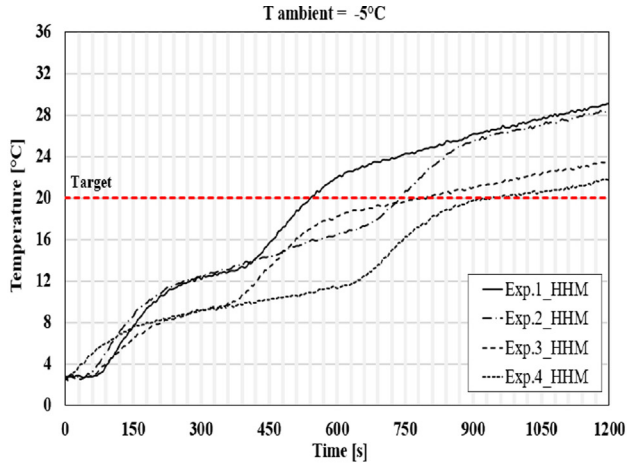


Fig. 10 **(a)** The temperature measurement data obtained for HHM heating mode at $T_{ambient}$ = -5 °C for the Exp_1 to Exp_4 **(b)** The temperature measurement data obtained for HHM heating mode at $T_{ambient}$ = -5 °C for the Exp_5 to Exp_8 **(c)** The calculated vehicle driving range and the measured temperature values at 1200 s of the heating period for HHM heating mode.

In the experiment of HHM_Exp_5, the maximum decrease in vehicle driving range was calculated about 72.3 % and the target temperature was achieved lower than 300 s. The temperature value was measured above the 30 °C in which 3 kW PTC heater and HP system worked together during the whole experiment and the calculated COP value was about 1.78.

From the results of the experiment of HHM_Exp_6, when the PTC capacity was selected as a value of 2 kW, the vehicle driving range was increased to about 77 % whereas the calculated COP value was reduced to 1.56 and the time to reach the target temperature was increased up to 785 s compared to the results of the experiment of HHM_Exp_5.

In the experiment of HHM_Exp_7 and HHM_Exp_8, only the PTC heater was activated as used in heating process of current electric vehicles. The results of the experiment of HHM_Exp_7 had similar performance with the results of HHM_Exp_6 in terms of getting target temperature, however, the COP was calculated lower than 1.0 in the experiment of HHM_Exp_7 and the time to reach the target temperature was increased up to 870 s. In the experiment of HHM_Exp_8, in which only 2 kW PTC heater was used, a maximum temperature value of 16 °C was observed and this value is much lower than the desired levels.

As a result, the heating modes such as MHM_1, MHM_2 and HHM with using Heat Pump system showed better performance compared to the experiments of HHM_Exp_7 and HHM_Exp_8 which used PTC component as a heating source. The thermal performance of all modes were evaluated in terms of heating process of hybrid heat pump system. On the other hand, the thermal performance of defogging/dehumidification process of EV HVAC system is very crucial for driver visibility and safety, in this paper, the defogging functions of HVAC system was not considered in the experimental studies, the thermal performance of HHPS during defogging/dehumidification will be studied considering driver safety, thermal comfort and also energy consumption in further studies.

The temperature values obtained from the experiments of all heating modes developed in this study are presented in Fig. 11 and Fig. 12 for different ambient conditions such as 0 °C and 5 °C, respectively. The target temperature was assumed as 20 °C for T = -5°C and this value was assumed as 25 °C for T = 0 °C and 30 °C for T = 5 °C so that the temperature difference was equal for all ambient conditions to get comparative results.

From the results of all heating modes, the temperature measurement values had similar tendency with the results of T = -5°C ambient conditions, however, the obtained temperature values were higher than the values obtained for lower ambient conditions. In the experiments of MHM_1, the measured temperature values were exceeded to 32 °C for T = 5 °C and this value was about 40 °C in the experiments of both MHM_2 and HHM.

The calculated COP values increased up to 2.5 and this value was the highest one in all experiments. These calculated COP values were compatible with the COP values available in the literature.

To evaluate the flow and the thermal characteristics of the vehicle cabin in different aspects, virtual points in different locations and vertical symmetry plane were defined and the numerical results were compared to the experimental results.

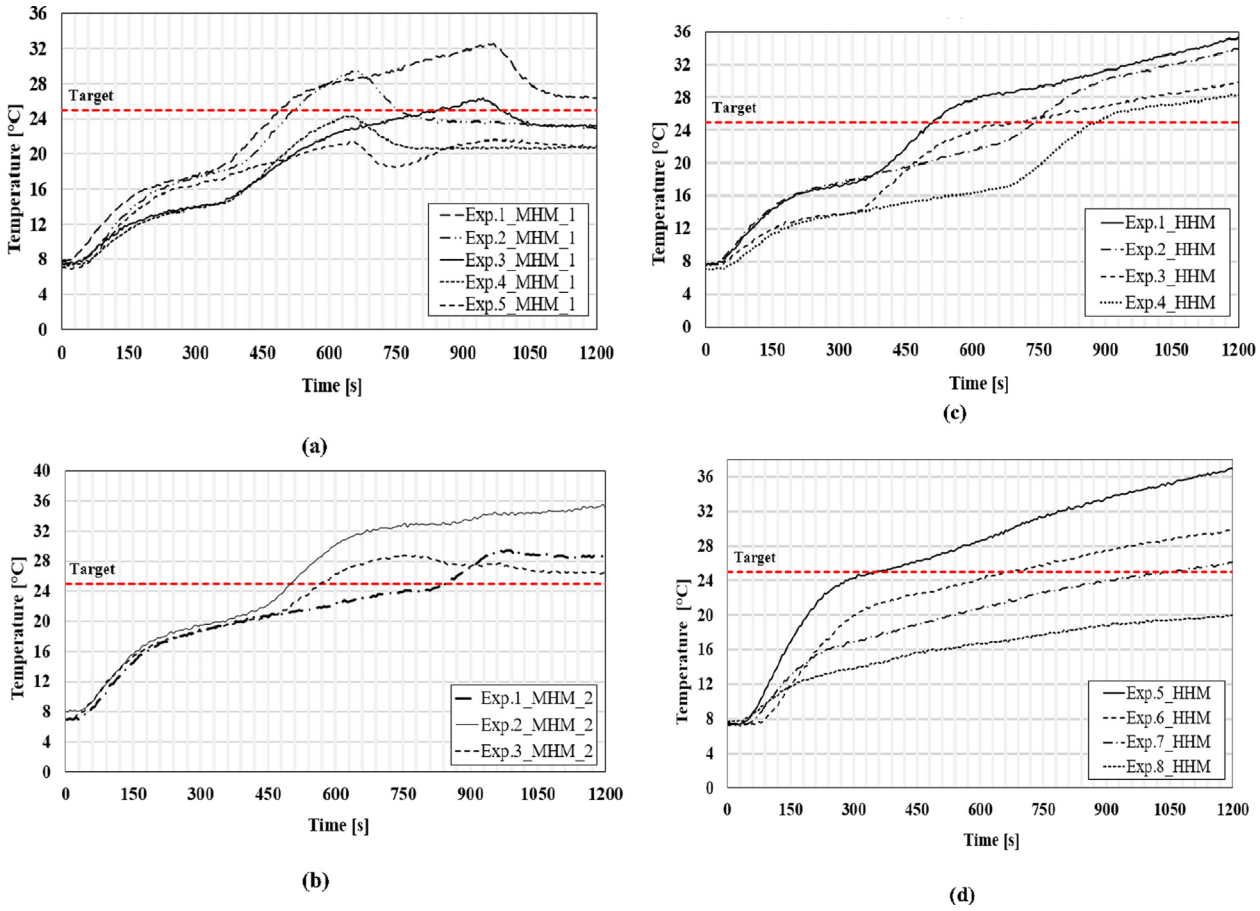


Fig. 11 The temperature measurement data obtained for MHM_1 heating mode at $T_{ambient}$ = 0 °C.

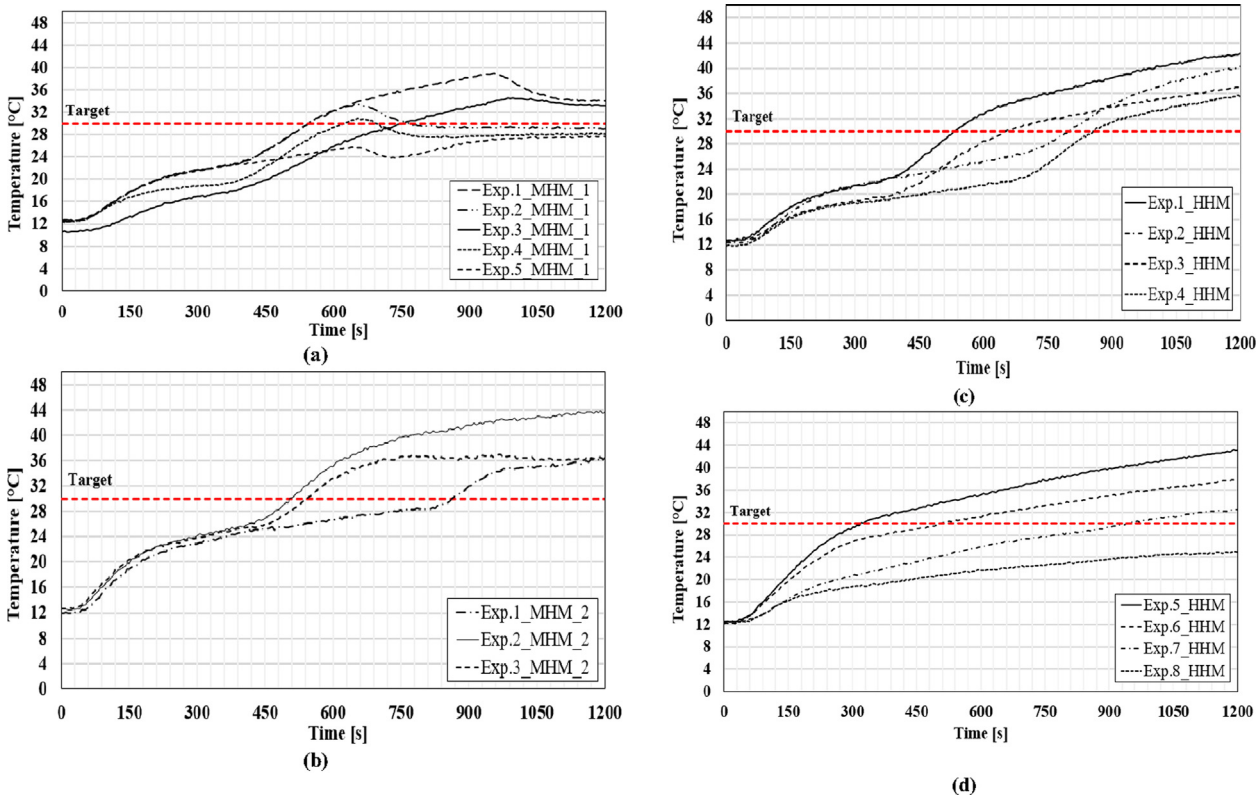


Fig. 12 The temperature measurement data for HHM heating mode at $T_{ambient}$ = 5 °C.

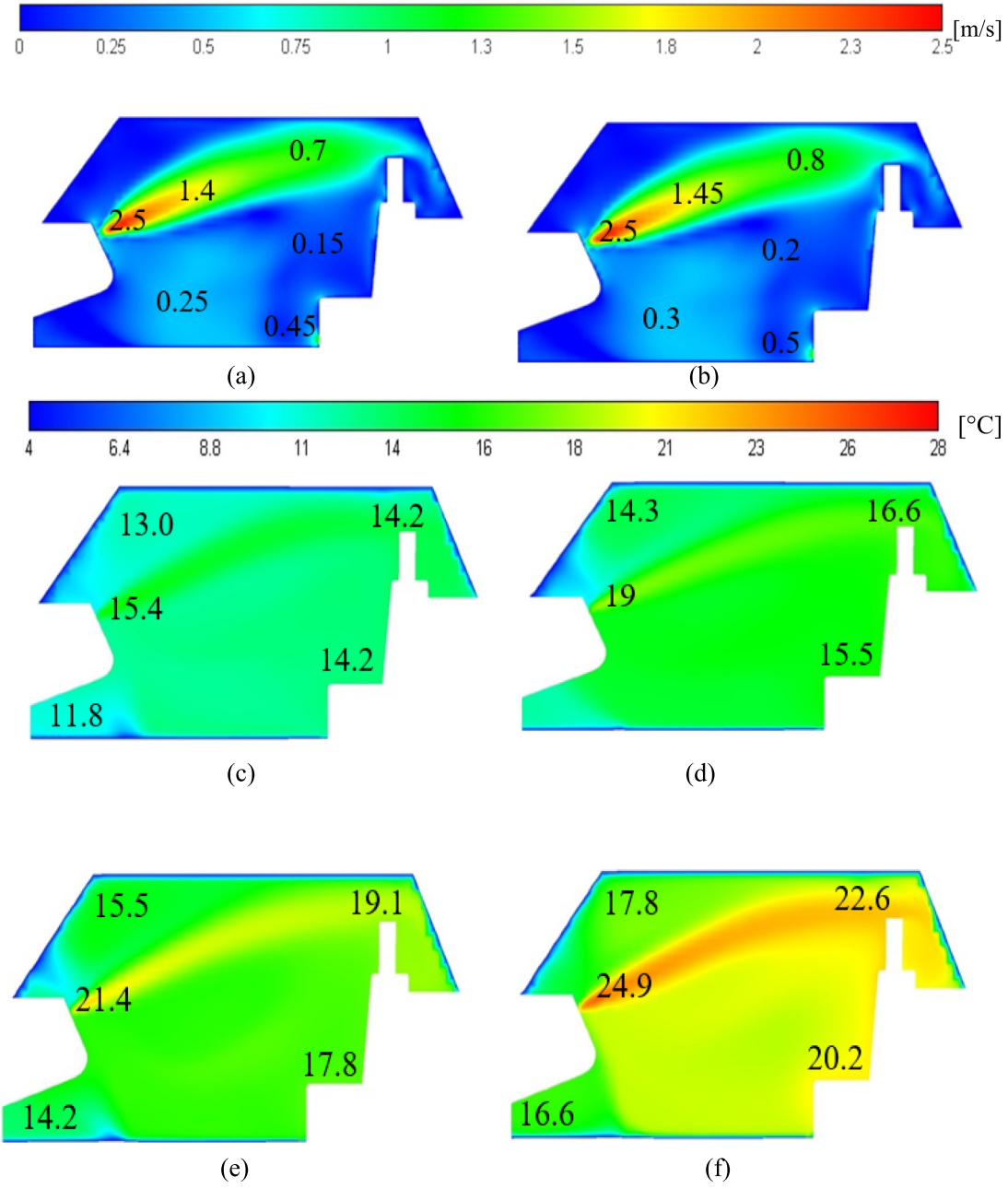


Fig. 13 **(a)** Velocity [m/s] distributions at the vehicle symmetry plane for t = 600 s of heating period and **(b)** for t = 1200 s of heating period **(c)** The predicted temperature values at the vehicle center plane during heating period.

The temperature distribution predicted on the symmetry plane of the vehicle cabin interior are demonstrated in Fig. 13. The velocity distribution of the vertical symmetry plane of the EVs cabin at 600 and 1200 s of heating periods are shown in Fig. 13a and Fig. 13b. At 1200 s of heating period, the maximum air velocity was computed near the inlet vent(s) and it was about 2.5 m/s. In accordance with flow direction this value was decreased to 0.5 m/s in the rear part of the cabin interior at that time. In the front region of the vertical plane of the vehicle cabin, velocity values changed between 0.25 and 2.5 m/s while in the back region of this plane these values ranged from 0.1 to 0.5 m/s, in general.

From the comparison of the velocity distributions, at 600 and 1200 s of heating periods, the velocity values computed for similar locations at the vertical plane were changed slightly thus we conclude that the steady-state conditions were reached at 600 s of heating period. As a result of velocity computations in vehicle cabin interior, a highly transient conditions were occurred in in 600 s heating period which is compatible with current literature [39–41].

The temperature distribution on the vertical symmetry plane during heating period is demonstrated in Fig. 13c-Fig. 13f. From the numerical results, the calculated temperature values at the beginning of the heating period, the temperatures inside the cabin model were quite low and the maximum temperature was about 15.4 °C. The higher temperature values were computed near the inlet vent(s) in general and this value was predicted about 25° at the end of the heating period. The computed local temperature values changed between 17 °C and 25 °C at that time. The lower temperature values were observed in the vehicle cabin at bottom and glass surfaces due to heat losses and another important result is that non-uniform air temperature distribution was obtained for the vertical symmetry plane of the vehicle cabin during heating period.

4. Conclusions

In this paper, both numerical and experimental results were presented for the evaluation of the energy consumption and also driving range to reach the desired temperature. Three different heating modes named as MHM_1, MHM_2, and HHM were investigated.

At lower ambient conditions such as T = -5°C, the experiment of MHM_1 had better performance in terms of energy consumption so that the calculated COP value was about 2.02 and the driving range was reduced to 77 %. However, MHM_2_Exp_3 had higher heating performance than the experiment of MHM_1 in terms of driving range and the calculated COP values were also similar. Another important result of the experiments of MHM_2, all experiments provided the target temperature at the end of the heating period. MHM_2_Exp_3 can be preferred for heating process especially at lower ambient temperature conditions while considering driving range and also energy consumption.

In the experiments of HHM, in general the higher temperature values were achieved by using PTC heater with HP system and the target temperature was obtained lower than 300 s but the maximum decrease in the driving range was obtained as a value of 71 % for this heating mode. In the experiment of HHM_Exp_4 case, the driving range was calculated for this experiment about 81.3 %. This means that the driving range of electric vehicle can be increased up to 15 % by using different heating modes of HHPS developed in this study. From the experimental results of all heating modes developed for different ambient conditions, in the experiments of MHM_1, the measured temperature values were exceeded to 32 °C for T = 5 °C ambient temperature and this value was about 40 °C in the experiments of both MHM_2 and HHM.

In general, the heating modes included Heat Pump system showed better performance compared to the experiments of HHM_Exp_7 and HHM_Exp_8 which used PTC component only as a heating source. In order to reach the desired temperature and driving range considering the target time, a high-capacity PTC heater and HP should be work together at the beginning of the experiment, and then the PTC capacity should be reduced gradually while the HP is operating without any change.

In this study, the major findings and conclusions are as follows.

(1) The driving range of electric vehicle can be increased up to 15 % by using different heating modes of HHPS included PTC heater and HP system developed in this study.
(2) To reduce the energy required for heating, hybrid heat pump system represent a promising solution for the new generation electric vehicles that the target temperature was obtained lower than 300 s by using PTC heater integrated with HP system at lower ambient conditions.
(3) The calculated COP values increased up to 2.5 and this value was the highest one in all experiments. These calculated COP values were compatible with the COP values which were in the available literature.
(4) Air temperature predictions were in good agreement with the experimental data in general. The higher temperature values were computed near the inlet vent(s) in general and this value was predicted about 25° at the end of the heating period. The computed local temperature values changed between 17 °C and 25 °C at that time and highly transient conditions were occurred in in 600 s heating period.

Declaration of Competing Interest

The authors declare that they have no known competing financial interests or personal relationships that could have appeared to influence the work reported in this paper.

Acknowledgement

The authors wish to thank the Scientific and Technological Research Council of Turkey (TUBITAK) for supporting this research under the project number 219 M475- TÜBİTAK 1001.

References

[1] J.T. Lee, S. Kwon, Y. Lim, M.S. Chon, D. Kim, Effect of air-conditioning on driving range of electric vehicle for various driving modes, in: SAE Technical Paper. (2013).
[2] K. Li, S. Luo, L. Fan, S. Hu, X. Zhou, R. Tu, H. Zhang, X. Jin, X. Zhao, L. Su, Investigation on the performance and characteristics of a heat pump system for electric vehicles under extreme temperature conditions, Case Studies in Thermal Engineering. 27 (2021) 101308.
[3] Z. Tian, W. Gan, X. Zhang, B. Gu, Y.L. Lin, Investigation on an integrated thermal management system with batter cooling and motor waste heat recovery for electric vehicle, Appl. Therm. Eng. 136 (2018) 16–27.
[4] F. Qin, Q. Xue, G.M.A. Velez, G. Zhang, H. Zou, C. Tian, Experimental investigation on heating performance of heat pump for electric vehicles at -20○C ambient temperature, Energy Convers. Manag. 102 (2015) 39–49.
[5] H. Zou, W. Wang, G. Zhang, F. Qin, C. Tian, Y. Yan, Experimental investigation on an integrated thermal management system with heat pipe heat exchanger for electric vehicle, Energy Convers. Manag. 118 (2016) 88–95.
[6] Z. Zhang, J. Wang, F. Xu, C. Li, Y. Chen, X. Wang, The solutions to electric vehicle air conditioning systems: a review, Renew. Sustain. Energy Rev. 91 (2018) 443–463.
[7] H. Bayram, G. Sevilgen, Thermal analysis of different heat pump systems for heating process of electric vehicles, Heat transfer research. 52 (6) (2021) 41–57.
[8] Q. Wang, B. Jiang, B. Li, Y. Yan, A critical review of thermal management models and solutions of lithium-ion batteries for

the development of pure electric vehicles, Renew. Sustain. Energy Rev. 64 (2016) 106–128.
[9] D. Chen, J. Jiang, G.-H. Kim, C. Yang, A. Pesaran, Comparison of different cooling methods for lithium ion battery cells, Appl. Therm. Eng. 94 (2016) 846–854.
[10] S. Panchal, R. Khasow, I. Dincer, M. Agelin-Chaab, R. Fraser, M. Fowler, Thermal design and simulation of mini-channel cold plate for water cooled large sized prismatic lithium-ion battery, Appl. Therm. Eng. 122 (2017) 80–90.
[11] E. Bulut, E.İ. Albak, G. Sevilgen, F. Öztürk, A new approach for battery thermal management system design based on Grey Relational Analysis and Latin Hypercube Sampling, Case Stud. Therm. Eng. 28 (2021) 101452.
[12] E. Bulut, E.İ. Albak, G. Sevilgen, F. Öztürk, Multi-Objective Optimization of Liquid Cooling System for a Twelve-Cell Battery Module, Heat Transfer Research. 53 (4) (2022) 15–31.
[13] E. Bulut, E.İ. Albak, G. Sevilgen, F. Öztürk, Prediction and optimization of the design decisions of liquid cooling systems of battery modules using artificial neural networks, Int. J. Energy Res. 46 (6) (2022) 7293–7308.
[14] S. Lee, Y. Chung, Y. Jeong, M.S. Kim, Experimental study on an electric vehicle heat pump system with multi-level waste heat recovery using a vapor injection technique at low ambient temperatures, Energy Convers. Manage. 267 (2002) 115935.
[15] H. Lee, D. Lee, Y. Kim, Heating performance of a coolant-source heat pump using waste heat from stack and electric devices in fuel cell electric vehicles under cold conditions, Energy Convers. Manage. 252 (2022) 115092.
[16] S. Lee, Y. Chung, Y. Jeong, M.S. Kim, Investigation on the performance enhancement of electric vehicle heat pump system with air-to-air regenerative heat exchanger in cold condition, Sustain. Energy Technol. Assess. 50 (2022) 101791.
[17] H. Ayartürk, E. Doruk, İ. Durgun, K. Ekbiç, New heating system development working with waste heat for electric vehicles, Transp. Res. Procedia 14 (2016) 1080–1086.
[18] F. Liu, F. Lan, J. Chen, Dynamic thermal characteristics of heat pipe via segmented thermal resistance model for electric vehicle battery cooling, J. Power Sources. 321 (2016) 57–70.
[19] T. Davin, J. Pellé, S. Harmand, R. Yu, Experimental study of oil cooling systems for electric motors, Appl. Therm. Eng. 75 (2015) 1–13.
[20] Z. Wang, M. Wei, C. Guo, M. Zhao, Enhance the heating performance of an electric vehicle AC/HP system under low temperature, Energy Procedia 105 (2017) 2384–2389.
[21] Q. Peng, Q. Du, Progress in heat pump air conditioning systems for electric vehicles—a review, Energies 9 (4) (2016) 240.
[22] Park, H. S., Development of the Waste Heat Management System (No. 2015-01-1605). SAE Technical Paper. (2015).
[23] Y. Lee, D. Jung, A Brief Performance Comparison of R1234yf and R134a in a Bench Tester for Automobile Applications, Appl. Therm. Eng. 35 (2012) 240–242.
[24] W. Li, R. Liu, Y. Liu, D. Wang, J. Shi, J. Chen, Performance Evaluation of R1234yf Heat Pump System for an Electric Vehicle in Cold Climate, Int. J. Refrig. 115 (2020) 117–125.
[25] H. Bayram, G. Sevilgen, M. Kılıç, Advances on Heat Pump Applications for Electric Vehicles, Adv. Auto. Eng. 1 (1) (2018) 79–104.
[26] A. Kabanovs, A. Garmory, M. Passmore, A. Gaylard, Computational simulations of unsteady flow field and spray impingement on a simplified automotive geometry, J. Wind Eng. Ind. Aerodyn. 171 (2017) 178–195.
[27] H. Zhang, L. Dai, G. Xu, Y. Li, W. Chen, W.Q. Tao, Studies of air-flow and temperature fields inside a passenger compartment for improving thermal comfort and saving energy. Part I: Test/numerical model and validation, Appl. Therm. Eng. 29 (10) (2009) 2022–2027.
[28] G. Sevilgen, M. Kilic, Investigation of transient cooling of an automobile cabin with a virtual manikin under solar radiation, Therm. Sci. 17 (2) (2013) 397–406.
[29] M.S.M. Ali, J. Jalasabri, A.M. Sood, S. Mansor, H. Shaharuddin, S. Muhamad, Wind noise from A-pillar and side view mirror of a realistic generic car model, DriAver, Int. J. Veh. Noise Vib. 14 (1) (2018) 38–61.
[30] K.Y. Kim, S.C. Kim, M.S. Kim, Experimental studies on the heating performance of the PTC heater and heat pump combined system in fuel cells and electric vehicles, Int. J. Automot. Technol. 13 (6) (2012) 971–977.
[31] X. Wu, D. Freese, A. Cabrera, W.A. Kitch, Electric vehicles' energy consumption measurement and estimation, Transp. Res. Part D: Transp. Environ. 34 (2015) 52–67.
[32] G. Sevilgen, M. Kilic, M. Aktaş, Dual-separated cooling channel performance evaluation for high-power led Pcb in automotive headlight, Case Stud. Therm. Eng. 25 (2021) 100985.
[33] Viscous Fluid Flow, Second Edition, Frank M. White, ISBN: 0-07-069712-4, 1991.
[34] Q. Chen, Comparison of different k-ε models for indoor air flow computations, Numer. Heat Transfer, Part B Fundam. 28 (3) (1995) 353–369.
[35] J.J. Costa, L.A. Oliveira, D. Blay, Test of several versions for the k–ε type turbulence modelling of internal mixed convection flows, Int. J. Heat Mass Transf. 42 (23) (1999) 4391–4409.
[36] M. Kilic, G. Sevilgen, Modelling airflow, heat transfer and moisture transport around a standing human body by computational fluid dynamics, Int. Commun. Heat Mass Transfer 35 (9) (2008) 1159–1164.
[37] M. Kilic, G. Sevilgen, Evaluation of heat transfer characteristics in an automobile cabin with a virtual manikin during heating period, Numerical Heat Transfer, Part A: Applications. 56 (6) (2009) 515–539.
[38] ANSYS Fluent 17.1 (2016) Theory Guide, ANSYS, Inc. USA.
[39] ASHRAE 1992. Thermal environmental conditions for human occupancy, ANSI/ASHRAE Standard 55-1992.
[40] M. Kılıç, G. Sevilgen, Evaluation of Heat Transfer Characteristics In An Automobile Cabin With A Virtual Manikin During Heating Period, Numer. Heat Transfer Part A-App. 56 (2009) 515–539.
[41] M. Kılıç, G. Sevilgen, The effects of using different type of inlet vents on the thermal characteristics of the automobile cabin and the human body during cooling period, Int. J. Adv. Manuf. Technol. 60 (2012) 799–809.
[42] G. Sevilgen, M. Kilic, Three dimensional numerical analysis of temperature distribution in an automobile cabin, Therm. Sci. 16 (1) (2012) 321–326.
[43] R.J. Moffat, Describing the uncertainties in experimental results, Exp. Therm Fluid Sci. 1 (1988) 3–17.
[44] L.B. Tan, Y.J. Yuan, Computational fluid dynamics simulation and performance optimization of an electrical vehicle Air-conditioning system, Alex. Eng. J. 61 (1) (2022) 315–328.
[45] T.B. Chang, J.J. Sheu, J.W. Huang, High-Efficiency HVAC System with Defog/Dehumidification Function for Electric Vehicles, Energies 14 (1) (2021) 3–12.
[46] Y. Yang, Y.O. Huang, J.S. Zhao, Optimization of the automotive air conditioning strategy based on the study of dewing phenomenon and defogging progress, Appl. Therm. Eng. 169 (2020) 114932.
[47] S. Na, M. Kim, M.S. Kim, Performance analysis of an automotive heat pump system with desiccant coated heat exchangers, Appl. Therm. Eng. 213 (2022) 118723.
[48] Mao Y.., Wang J., Li J., Experimental and numerical study of air flow and temperature variations in an electric vehicle cabin during cooling and heating, Applied Thermal Engineering, (2018), 356-367.